INDIAN JOURNAL OF SCIENCE AND TECHNOLOGY

RESEARCH ARTICLE

Impact of CC and PCTIG Welding on SMO 254 Joints Using Alloy 625 Filler

P John Raj Kumar[1]*, A Baskaran[2]

1 Research Scholar, Department of Manufacturing Engineering, Annamalai University, Chidambaram, 608002, Tamil Nadu, India
2 Assistant Professor, Department of Manufacturing Engineering, Annamalai University, Chidambaram, 608002, Tamil Nadu, India

OPEN ACCESS

Received: 25-07-2024

Accepted: 16-08-2024

Published: 27-08-2024

Citation: Kumar PJR, Baskaran A (2024) Impact of CC and PCTIG Welding on SMO 254 Joints Using Alloy 625 Filler. Indian Journal of Science and Technology 17(34): 3553-3566. https://doi.org/10.17485/IJST/v17i34.2163

* **Corresponding author**.

johnme1982@gmail.com

Funding: None

Competing Interests: None

Published By Indian Society for Education and Environment (iSee)

ISSN
Print: 0974-6846
Electronic: 0974-5645

Abstract

Objectives: This investigation analyzes the microstructure, mechanical and corrosion characteristics of SMO 254 joints welded using constant current TIG (CCTIG) and pulse current TIG (PCTIG) with alloy 625 (ERNiCrMo-3) filler metal. **Method:** Optical microscopy and SEM with EDAX were employed for microstructural characterization and phase analysis. Mechanical properties were assessed through Vickers microhardness, tensile, and Charpy impact tests, followed by fracture analysis. **Findings:** EDAX point analysis indicates reduced Mo segregation and the absence of Nb segregation in PCTIG weldments. The overall corrosion resistance remains acceptable despite a slightly higher corrosion rate in PCTIG weldments. The study highlights the superior mechanical properties and microstructural control achieved with PCTIG welding, making it a preferable technique for SMO 254 joints. **Novelty:** Notably, the research establishes PCTIG as a superior method for welding SMO 254, demonstrating that it not only refines the grain structure but also significantly enhances mechanical properties, particularly toughness, by 50% compared to CCTIG.

Keywords: SMO 254; SASS; Microstructural characterization; Mechanical properties; CCTIG; PCTIG

1 Introduction

Austenitic stainless steels exhibit superior resistance to corrosion and possess remarkable strength. 6% Moly alloys are frequently found to include significant amounts of Fe 53.42%, Ni 19.04%, Cr 19.88%, and N 0.199 %, which help them resist corrosion and stress cracking. Super austenitic stainless steel is used in pipelines, special tanks, pumps, power plant heat exchangers, paper, chemical, petrochemical, and flue gas desulfurization devices, and refining sectors. These alloys are part of the austenitic stainless steel family. Super austenitic stainless steels (SASS), also known as 6% moly alloys, are easily weldable, but the key challenges are preventing hot cracking and maintaining corrosion resistance. The standard grade of SASS is SMO 254, highly alloyed stainless steel that contains nickel, chromium, molybdenum, and nitrogen. SMO 254 stainless steel is prone to nickel, chromium, and, notably, molybdenum micro-segregation due to the primary austenitic solidification mode[(1)]. GTAW processes

provide several notable advantages, including ease of use, low cost, strong metallurgical connections between joints, attractive appearance, and enhanced weld properties[2]. Constant current GTAW process is commonly used in industry for welding different austenitic stainless steel. Current pulsing offers superior weld metal characteristics over constant current, including less heat input, improved weld bead geometry, increased arc stability, and decreased HAZ[3]. Segregation causes Mo depletion in the dendritic core, which is susceptible to corrosive attack. Localized corrosion can occur when a Ni-based filler metal forms an unmixed zone between a partly melted zone and a weld nugget[4]. With the 316L filler weld, Chetan[5] observed increased tension and toughness strengths and chromium carbide precipitate in the autogenous weld joint between 316L and 430 alloys. Autogenous welds exhibited greater pitting and sensitization. Using ERNiCrCoMo-01, ERNiCrMo-4, 10, and 14 fillers, Mahesh[6] studied alloy 617 joints by CCTIG welding. The authors discovered Mo-rich phases using fillers ERNiCrMo-4, 10 and 14 and cellular and columnar structures in the weld zone. They also identified Cr- rich phases in ERNiCrMo-1 filler metal. Yelamasetti[7] used continuous and pulsed TIG welding methods to examine the metallurgical and physical characteristics of weld joints of SS 316 and alloy 400. During a metallurgical examination, grain refinement was found in the PCTIG weldment at HAZ. Ultimate tensile strength was observed around 554 and 542 MPa in PCGTAW and CCGTAW weldments, respectively. PCTIG compared to CCTIG, the yield strength to UTS ratio is more excellent. Compared to CCTIG joint, the PCTIG joint is more complex. Yahya[8] examined Inconel 601 and 304 SS filler with continuous and pulse currents. Author noted absence of segregation in weld metal. Further there is improved grain refinement due to less heat input and this increased mechanical property of pulse weld joints. But solid and ductile autogenous welding is produced. Fahd[9] achieved complete penetration with reduced heat input in his investigation of the pulsing effect in titanium alloy welding, and weld metal had a higher tensile strength than base metal. The cause of grain strengthening is an increased cooling rate in the fusion zone. By using TIG welding to examine the effect of 310 Austenitic and 410 Ferritic stainless-steel fillers in 430 Ferritic stainless steel, Shanmugasundar[10] study revealed that filler metal influences dilution, Cr/Ni equivalent ratio, mechanical, metallurgical features. The literature survey underscores the well-established benefits of super austenitic stainless steels, particularly SMO 254, in terms of corrosion resistance and mechanical strength. Previous research has explored the challenges associated with welding super austenitic stainless steels (SASS), focusing on issues such as preventing hot cracking and maintaining corrosion resistance. This study addresses this gap by providing new insights into the effects of CCTIG and PCTIG on SMO 254 joints, offering novel findings on microstructural control, mechanical performance, and corrosion behavior.

2 Methodology

This investigation employed an SMO 254 plate, which is4 mm thick, as the base metal.ERNiCrMo-3 (alloy 625), having a 2.4 mm diameter, is the filler material utilized. A wire cut EDM machine cut four pieces of 50 x 45 x 4 mm. A single v-butt joint arrangement with a 3 mm root spacing, 1mm land and 60^0 included angles were used. Welding joints were made using a TIG 315 BP AC/DC machine in DCEN continuous and pulse current modes. A 2.4mm diameter non-consumable tungsten electrode with 2% thoriated was employed. The welding process was done manually. Table 1 lists the parameters for welding. Argon shields and purges gas during root and filling pass welding at a flow of 10 lpm. The microstructures of the three weld zones were inspected using an optical microscope and a FE-SEM. The physical characteristics of the weldments were determined by hardness, tension, and impact testing. Tensile testing was done according to ASTM E8 guidelines[11]. Weldment's hardness was assessed using micro Vickers tester at 0.5mm intervals, with a 1 kg force and 15 second dwell period. Non-standard Charpy impact test specimen's length 55 mm, width 10 mm and thickness 4 mm were used for comparison. A W-EDM machine used to cut the specimens to examine their mechanical and metallurgical properties. In CCTIG and PCTIG, heat input is determined by applying Equations (1), (2) and (3)[10]. Weld bead geometry measurements, such as bead width (w), bead height (h), and depth of penetration (t), were measured from both macro images of weld specimens using Image J software, and percentage dilution (D) were calculated by applying Equation (4).

$$HI_{CCTIG} = \eta\,(Vx\,I\,/S)\,in\,KJ\,/\,mm; \tag{1}$$

$$HI_{PCTIG} = \eta(Vx\,I_m/S)\,in\,KJ\,/\,mm\,; \tag{2}$$

$$I_m = \frac{t_p \times T_p + t_b \times T_b}{T_p + T_b}\ in\ Amps: \tag{3}$$

The TIG welding process efficiency is 60%. Other factors that affect the welding process include welding speed, S (mm/min), Voltage (V), I_p pulse current (amps), I_b base current (amps), T_p base current period (s) and T_p pulse current period (s).

Table 1. Experimental specifications used in CCTIG and PCTIG welding of SMO 254

Welding	Filler metal	Filler metal dia. (mm)	No. of pass	Welding current (A)	Base current I_b (A)	Peak current I_p (A)	Voltage (V)	Welding speed (mm/min)	Total heat input (KJ/mm)
CCTIG	ERNiCrMo-3	2.4	Root	123		-	10	78	
			Fill	123	-		10	78	1.136
PCTIG	ERNiCrMo-3	2.4	Root	123	63	120	10	78	
			Fill	123	63	120	10	78	1.136

3 Results and discussion

3.1. Microstructure evaluation

3.1.1. Dilution analysis

Percentage of dilution is one of the characteristics of weld joint. Dilution can be calculated by fused base metal area to the total weld metal area. Almost equal percent of dilution noted from both welding methods. Table 2 PCTIG welding shows marginally higher dilution percentage and lower penetration when compared with CCTIG welding.

$$Percentage\ Dilution\ (D)\ =\ Fused\ area\ of\ base\ metal\ /\ whole\ weld\ area \tag{4}$$

Table 2. Weld bead geometry and weld dilution

Welding method	Weld bead geometry in mm			Percentage Dilution (D) %
	Bead width (w)	Bead height (h)	Penetration (p)	
CCTIG	8.7	0.902	5.31	36.50
PCTIG	8.98	0.783	4.903	38

The bead geometry directly influences the dilution percentage. In the case of CCTIG welding, the bead width is slightly narrower (8.7 mm) compared to PCTIG welding (8.98 mm). The bead height in CCTIG is greater (0.902 mm) than that in PCTIG (0.783 mm), indicating a more pronounced buildup of weld metal above the base metal surface. However, the penetration depth is more significant in CCTIG (5.31 mm) than in PCTIG (4.903 mm), suggesting more profound fusion into the base metal. The higher penetration in CCTIG results in a more significant amount of base metal being melted and mixed with the filler metal, contributing to a substantial dilution percentage of 36.50%. Conversely, PCTIG, despite having a slightly broader bead width, exhibits reduced penetration. This reduced penetration limits the extent of base metal mixing with the filler metal, resulting in a somewhat higher dilution percentage of 38.00%.

The welding parameters, including welding current, voltage, and speed, play a pivotal role in determining the heat input and the weld bead geometry and dilution. In both CCTIG and PCTIG processes, the total heat input is maintained at 1.136 KJ/mm. However, the mode of current application differs significantly. CCTIG utilizes a continuous current of 123 A for both the root and fill passes. PCTIG employs a pulsed current with a peak current of 120 A and a base current of 63 A, maintaining the same average current as CCTIG but in a pulsed manner. The pulsed nature of PCTIG allows for periodic cooling during the welding process, which promotes grain refinement and reduces the overall heat input per unit time. This results in a finer microstructure and better mechanical properties, as observed in the increased toughness values. The reduced penetration in PCTIG can be attributed to the intermittent heat application, allowing the base metal to cool slightly between pulses, thereby limiting the depth of fusion [12].

The slight increase in dilution percentage for PCTIG (38.00%) compared to CCTIG (36.50%) can be attributed to the combined effect of bead width and penetration. While PCTIG offers a broader bead width, its reduced penetration limits the extent of base metal mixing. The interplay between these geometric factors and the pulsed current mode results in a controlled dilution, which is beneficial for maintaining the integrity and desired properties of the weld joint [13]. Furthermore, the findings suggest that while both welding techniques produce acceptable dilution levels, PCTIG provides superior control over the weld microstructure due to its reduced penetration and grain refinement capabilities.

3.1.2. Macroscopic Analysis

The macroscopic images of the weld joints created by Constant Current TIG (CCTIG) and Pulsed Current TIG (PCTIG) welding processes are depicted in Figure 1**(a)** and Figure 3 **(a),** respectively. These images provide a visual confirmation of the weld quality and the effectiveness of the welding parameters used in this study. The macro photos show that both welding techniques have produced weld joints with no visible defects such as cracks, porosity, or incomplete fusion. In CCTIG Welding, the macro image of the weld joint shows a well-defined bead with consistent width and height. The fusion zone appears uniform, indicating steady heat input and effective base metal fusion with the filler material. The two welding passes, root and fill, are distinguishable, each contributing to the overall integrity of the weld [(14)]. The macro image of the PCTIG weld joint also demonstrates a defect-free weld. However, compared to the CCTIG weld, the fusion zone in the PCTIG weld appears narrower. This is attributed to the pulsed current mode, which allows for better control over the heat input and, consequently, a more concentrated fusion zone.

The narrower fusion zone observed in the PCTIG weld is a significant finding. The pulsed current technique facilitates periodic cooling during welding, which not only aids in grain refinement but also minimizes the heat-affected zone (HAZ). This controlled heat input results in a more precise and narrower fusion zone, which is advantageous for reducing thermal distortion and residual stresses in the weldment [(15)]. In contrast, the CCTIG weld, with its broader fusion zone, indicates a higher heat input over a continuous period. While this ensures thorough fusion and adequate mixing of the base and filler metals, it also results in a wider HAZ, potentially leading to higher residual stresses and distortion in the weldment.

The macroscopic analysis agrees with the findings from the dilution analysis. The narrower fusion zone in PCTIG welds, coupled with reduced penetration and controlled dilution, translates to improved mechanical properties such as higher toughness and better resistance to thermal stresses [(16)]. The grain refinement observed in the microstructural analysis further supports these findings, indicating that PCTIG welding not only refines the grain structure but also enhances the overall performance of the weld joint.

3.1.3. CCTIG weld using ERNiCrMo-3

Figure 1**(b)** and **(c)** provide detailed microstructural views of the SMO 254 similar weldment at the interface when subjected to Constant Current TIG (CCTIG) welding. This analysis reveals significant insights into the microstructural transformations and elemental segregation that occur during the welding process. The CCTIG process forms an unmixed zone (UMZ) at the weld interface, as depicted in Figure 1 **(c).** This UMZ is a narrow region adjacent to the fusion line where the base metal did not completely melt, yet experienced significant thermal cycles [(17)]. The presence of the UMZ indicates that while the base metal's microstructure remains essentially unchanged, it may undergo slight modifications due to the heat from the welding process.

In the weld metal, the microstructure is characterized by dendritic structures, as illustrated in Figure 1**(b)**. The primary dendritic arms are the main trunks of these structures, which form during the initial stages of solidification. These primary arms serve as the backbone for the secondary dendritic arms, which branch off and help in the redistribution of solute elements. The dendritic and inter-dendritic regions observed in the columnar grains further confirm the directional solidification pattern, typical in weld metals with steep temperature gradient [(18)].

Elemental micro-segregation is another significant observation in the CCTIG welds. Figure 1**(c)** and **(e)** highlight the presence of black and white patches, indicative of micro-segregation of alloying elements within the heat-affected zone (HAZ). This segregation results from the varying heating and cooling cycles during welding, which cause differential diffusion rates of elements like Mo and Nb. In the HAZ, the microstructure exhibits annealing twins, equiaxed grains, and epitaxial grain growth [(19)]. The annealing twins, typical in face-centered cubic (FCC) metals such as SMO 254, appear as mirror-image crystallographic features within the grains. These twins can influence the mechanical properties by interacting with dislocations and providing sites for stress relief. Equiaxed grains, which have nearly spherical shapes and uniform dimensions, are also evident in the HAZ. These grains form due to the uniform cooling rates in the central region of the weld pool, leading to random, non-directional grain growth [(20)]. The presence of epitaxial grain growth at the fusion boundary, where the new grains grow directly from the pre-existing grains of the base metal, maintains the crystallographic orientation of the parent grains, ensuring a seamless transition between the weld metal and the base metal [(21)].

The microstructural transformations observed in the CCTIG welds directly affect the mechanical properties of the welded joint. The formation of columnar structures and dendritic arms contributes to the strength and stability of the weld metal. However, elemental micro-segregation can lead to local variations in mechanical properties, potentially affecting the overall performance of the weld. The absence of migrated grain boundaries in the weld area, as noted in Figure 1**(e)** is a positive indicator of the weld's stability. Migrated grain boundaries can be sites for crack initiation and propagation, thus their absence enhances the weld's resistance to fracture.

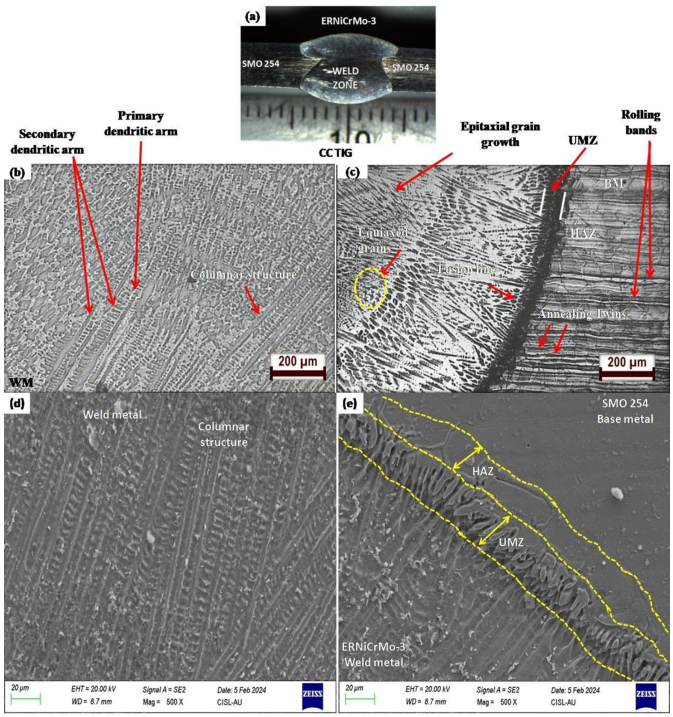

Fig 1. (a) Macrostructure of CCTIG (b) weld metal microstructure (c) ERNiCrMo-3 weld metal andSMO 254 base metal interface microstructure, SEM image of CCTIG (d) weld metal (e) weld interface

Figure 1**(c)** and **(e)** depict the interaction between the weldment and the base metal SMO 254. The microstructural analysis shows rolling bands in the base metal, which are elongated regions formed during the rolling process and exhibit different grain orientations and dislocation densities [21] [22]. These bands can influence the mechanical behavior of the base metal during welding. The fusion line, where the base metal begins to melt and mix with the weld metal, marks the transition from the solidified base metal to the weld metal. The epitaxial grain growth observed at this boundary ensures a robust metallurgical bond, enhancing the integrity of the weld joint.

The FE SEM combined with EDAX provides a comprehensive understanding of the elemental composition and distribution within the CCTIG weldment. The detailed analysis at the weld fusion zone is depicted in Figure 2**(a),** revealing critical insights into the microstructural and compositional characteristics of the weldment. The EDAX analysis indicates that the primary constituents of the weld dendritic core are Ni, Nb, Cr, Fe, and Mo. These elements are integral to the weld metal's properties, contributing to the overall mechanical strength and corrosion resistance. The dendritic core, formed during solidification, shows a homogeneous distribution of these elements, ensuring a stable and robust microstructure. In contrast, the inter-dendritic regions exhibit variations in elemental concentrations. Specifically, higher quantities of Fe, Ni, Mo, and Cr are detected in these areas [23]. This segregation results from the differential solidification rates during the welding process, where elements with lower melting points and higher diffusivity tend to migrate to the inter-dendritic spaces. The EDAX point scan reveals significant Nb and Mo segregations at the grain boundaries.

The EDAX line scans, as shown in Figure 2**(b),** provide a detailed view of the elemental transition across the weld fusion zone. These scans illustrate the gradual changes in elemental concentrations, reflecting the diffusion processes occurring during welding. The transition of elements such as Cr, Ni, and Mo from the base metal (BM) to the weld metal (WM) is particularly notable. This transition is more pronounced in the SMO 254 base metal to weld metal interface due to the alloy's increased thermal diffusivity and thermal conductivity. The higher thermal conductivity of the ERNiCrMo-3 filler metal enhances the heat flow during welding, promoting the diffusion of alloying elements [24]. The microstructural analysis correlates well with the elemental distribution observed in the FE SEM with EDAX analysis. The presence of dendritic and inter-dendritic regions and elemental segregation at grain boundaries indicate the solidification dynamics during the CCTIG welding process. The primary and secondary dendritic arms observed in the SEM images Figure 1 **(d),** is composed of a homogeneous distribution of Ni, Nb, Cr, Fe, and Mo, ensuring the structural integrity of the weldment [25].

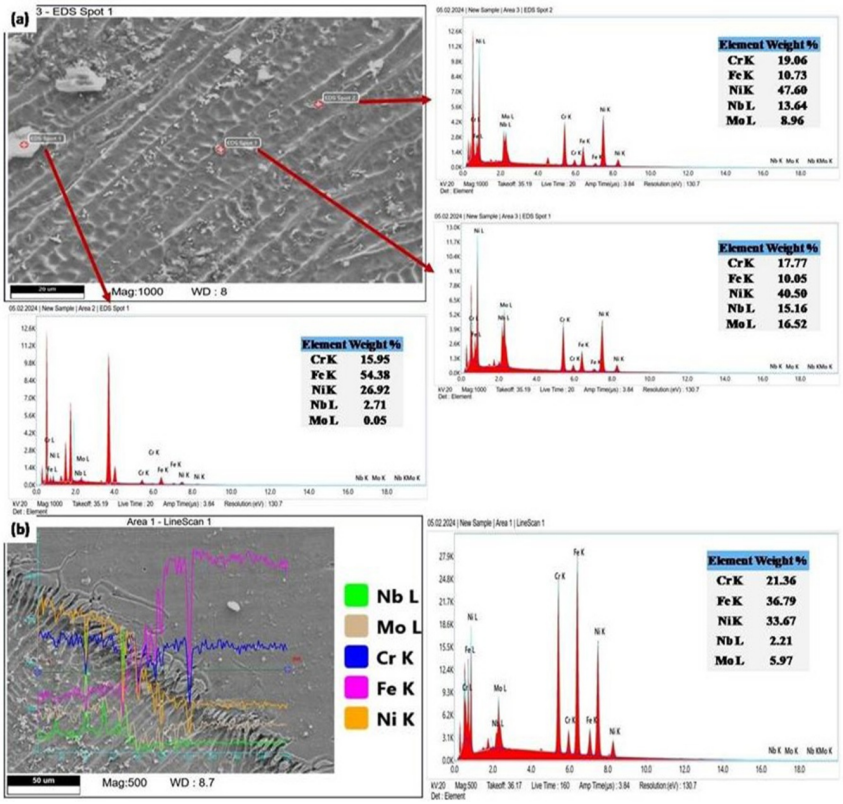

Fig 2. (a) EDAX point analysis on dendritic and interdendritic regions of CCTIG weld metal (b) EDAX line analysis in weld metal interface of CCTIG

However, the segregation of Nb and Mo at grain boundaries, as revealed by EDAX point scans, can impact the mechanical properties. These segregated areas might exhibit different hardness and tensile strength than the dendritic core, potentially leading to localized weaknesses. The elemental transitions captured by the EDAX line scans reflect the diffusion of key alloying elements from the base metal to the weld metal. This diffusion is crucial for achieving a strong metallurgical bond and ensuring the overall performance of the weldment [26]. The increased thermal diffusivity of the SMO 254 alloy, combined with the thermal conductivity of the ERNiCrMo-3 filler, facilitates effective diffusion and alloying at the weld interface.

The elemental composition and segregation patterns also have significant implications for the corrosion resistance of the weldment. Cr and Mo, known for their corrosion resistance properties, are crucial in both the dendritic core and inter-dendritic regions. However, the segregation of these elements at grain boundaries can create sites susceptible to localized corrosion, particularly in aggressive environments [27]. The transition and distribution of Cr, Ni, and Mo from the base metal to the weld metal enhance the overall corrosion resistance of the weldment.

3.1.4. PCTIG weld using ERNiCrMo-3

The microstructural analysis of the Pulsed Current TIG (PCTIG) weldment reveals significant insights into the effects of regulated heat input and pulse frequency on the weld microstructure. As shown in Figure 3 **(b)**, the regulated heat input and appropriate pulse frequency employed during PCTIG welding significantly reduce the formation of coarse grain structures in the SMO 254 weld metal. The presence of a fine-grained microstructure enhances the mechanical properties of the weld by improving toughness and reducing the likelihood of crack propagation. The controlled pulse frequency allows for periodic cooling, which helps refine the grain size by preventing excessive growth.

Adjacent to the weld interface, the SEM image inFigure 3**(c)** reveals the presence of a narrow Unmixed Zone (UMZ). The appropriate pulse frequency and regulated heat input are crucial in maintaining this narrow UMZ, which ensures minimal disruption to the base metal while achieving sufficient fusion. The narrow UMZ indicates that the base metal experienced significant heating without melting, preserving its original microstructure and mechanical properties to a large extent. The lengthy columnar dendritic structure, as observed on the weld metal side next to the weld interface in Figure 3 **(b),** is indicative

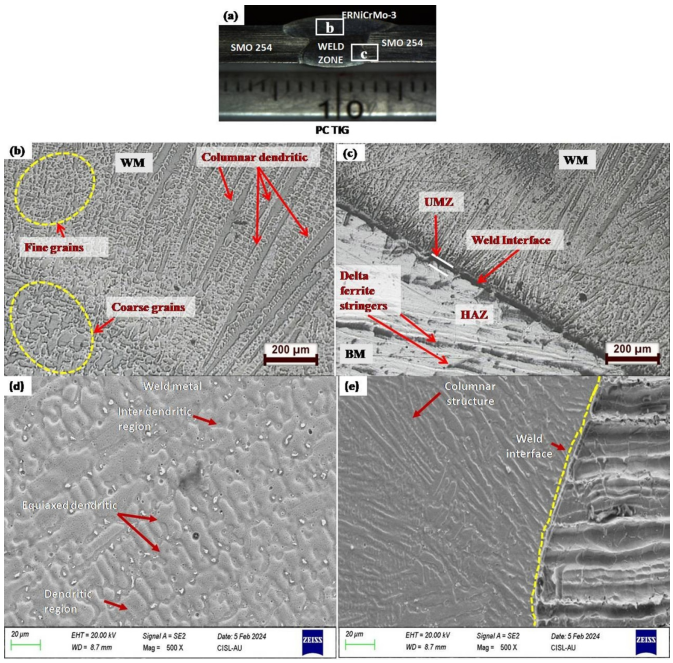

Fig 3. (a) Macrostructure of PCTIG (b) weld metal microstructure (c) weld metal and base metal interface microstructure, FESEM image of PCTIG (d) weld metal (e) weld interface

of directional solidification. The steep temperature gradient near the weld interface promotes the growth of elongated, columnar dendrites. These columnar structures are essential for the stability of the weld metal, providing a solid foundation for the subsequent layers of material.

Figure 3**(d)** shows an equiaxed dendritic structure in the dendritic region. Refined equiaxed grains can be formed due to cyclic heating and cooling during the PCTIG welding process. This cyclical thermal regime disrupts the growth of large columnar grains, instead promoting the nucleation and growth of smaller, equiaxed grains. The presence of Ni in the dendritic region further enhances the mechanical properties by contributing to the strength and corrosion resistance of the weld meta [28]. The weld interface, depicted in Figure 3 **(e),** shows a well-defined columnar structure, highlighting the transition between the weld metal and the base metal. The columnar grains grow epitaxially from the base metal grains, ensuring a seamless metallurgical bond. This epitaxial growth is crucial for maintaining the continuity of the microstructure across the weld interface, which is vital for the overall strength and integrity of the weldment [29].

The controlled heat input and pulse frequency during PCTIG welding play a pivotal role in determining the microstructural characteristics of the weldment. By carefully regulating these parameters, achieving a balance between sufficient fusion and minimal heat-affected zone (HAZ) width is possible. This balance ensures that the weld metal possesses a refined microstructure with improved mechanical properties. The fine equiaxed grains observed inFigure 3**(d)** and the narrow UMZ shown in Figure 3 **(c)** are direct results of the cyclic heating and cooling provided by the pulsed current [30]. The refined microstructure observed in the PCTIG weldment directly correlates with improved mechanical properties. The reduction in coarse grains and the presence of fine equiaxed grains contribute to higher toughness and better resistance to thermal and mechanical stresses [31].

Figure 4**(b)** illustrates the FE SEM/EDAX line scan across the weld metal interface of the PCTIG weldment. This line scan provides a comprehensive view of the elemental distribution from the base metal (BM) through the heat-affected zone (HAZ) and into the weld metal (WM). The distribution of Fe, Ni, Cr, and Mo elements is clearly delineated, confirming their presence throughout these regions. The line scan reveals a gradual transition of elements across the weld interface, with a noticeable concentration of Fe migrating from the SMO 254 base metal towards the fusion zone. This migration contributes to the formation of the lengthy columnar dendritic structure near the weld zone, as observed in the microstructural analysis. These columnar dendrites, characterized by their elongated grain structure, indicate directional solidification influenced by the thermal gradient during welding.

The absence of Nb segregation further ensures uniformity in the weld metal, reducing the risk of localized weaknesses. The elemental transition across the weld interface, particularly the movement of Fe from the base metal to the fusion zone, plays a

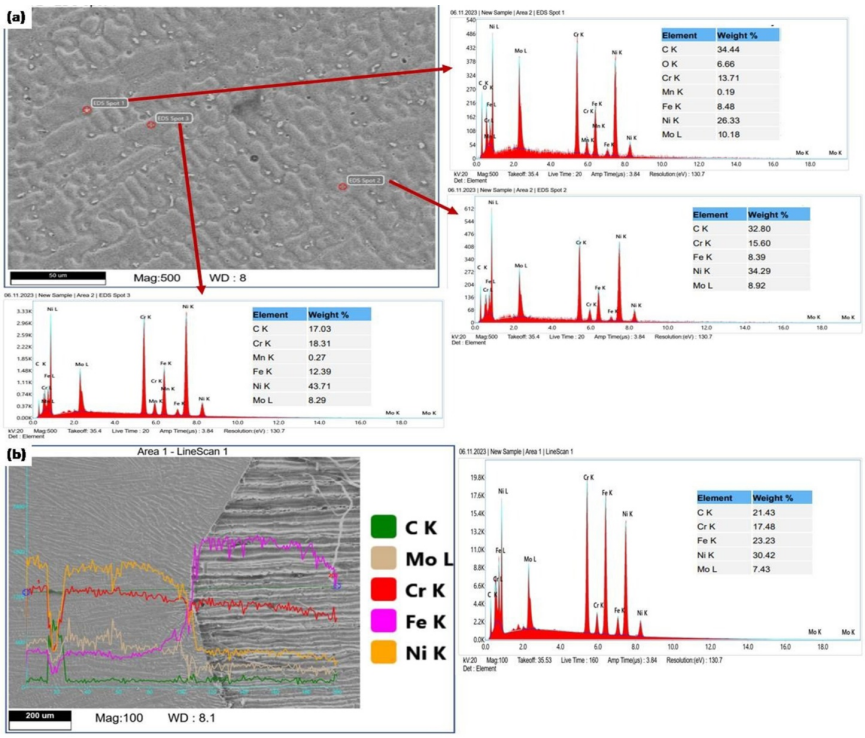

Fig 4. (a) EDAX point analysis on dendritic and interdendritic regions of PCTIG weld metal (b) EDAX line analysis in weld metal interface of PCTIG

crucial role in forming the columnar dendritic structure. These columnar dendrites provide a strong foundation for the weld metal, contributing to its mechanical strength and stability

Figure 4**(a)** presents the SEM/EDAX analysis at the weld metal, highlighting the enrichment of critical alloying elements such as Ni, Cr, Fe, C, and Mo. The EDAX spectra show pronounced peaks for these elements, indicating their significant presence within the weld metal. Nickel (Ni), the primary alloying element, is particularly noteworthy. Its high concentration contributes to forming a fully austenitic phase structure, as corroborated by the equiaxed dendritic structure seen in Figure 3 **(d)**. This austenitic structure enhances the weld metal's toughness and corrosion resistance. The absence of Nb (Niobium) segregation at the grain boundaries, as revealed by the EDAX point scan, indicates the uniform distribution of alloying elements. Nb segregation can lead to localized weaknesses and susceptibility to cracking; hence, its absence suggests a more homogeneous and robust weld metal.

3.2. Mechanical Behavior

3.2.1. Micro-hardness properties

Microhardness measurements were performed on the weldments created by Constant Current TIG (CCTIG) and Pulsed Current TIG (PCTIG) welding techniques in three distinct areas: the weld zone's top, middle, and bottom. The result, shown inFigure 5**(a)** and Figure 5 **(b)** for CCTIG weldment, the corresponding weld zone average microhardness was observed to be 218.66, 222.86, and 212.06 HV in the top, middle, and bottom. The microhardness distribution in the CCTIG weldment indicates relatively consistent hardness values across the weld zone, with a slight decrease in the bottom region[32]. This distribution suggests a uniform microstructure with minor variations in grain size and elemental composition throughout the weldment. The consistent hardness values can be attributed to the continuous heat input and steady cooling rate characteristic of CCTIG welding, which promotes uniform grain growth and elemental distribution.

For the PCTIG weldment, the average microhardness values observed were 221.73 HV in the top, 224.3 HV in the middle and 265.46 HV in bottom. In contrast to the CCTIG weldment, the PCTIG weldment exhibits a significantly higher microhardness in the bottom region. This improved hardness profile can be attributed to the reduced heat input and increased rate of weld pool cooling associated with the pulsed current technique. The current pulsing effect induces cyclic heating and cooling, enhancing

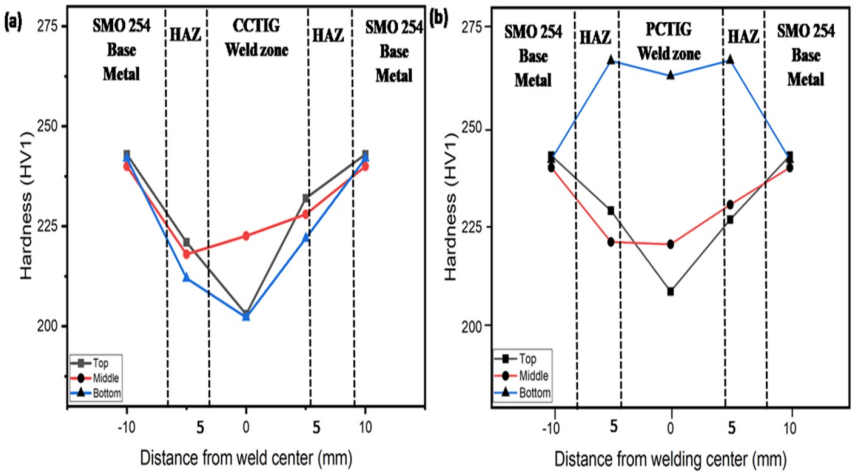

Fig 5. Microhardness of the welded joints (a) CCTIG (b) P CTIG

the solidification rate and promoting finer grains' formation in the microstructure [33]. The rapid cooling in the PCTIG weldment results in a refined microstructure with reduced grain size, particularly in the bottom region where the cooling rate is highest. The finer grains contribute to the increased hardness observed in this area.

The variations in microhardness between the CCTIG and PCTIG weldments are closely correlated with their respective microstructures and diffusion characteristics. In CCTIG welding, the continuous heat input leads to a more uniform grain structure with minor differences in hardness across the weld zone. The steady cooling rate allows for gradual solidification, resulting in consistent microhardness values. In PCTIG welding, the pulsed current induces rapid thermal cycles, significantly affecting microstructural evolution and elemental diffusion. The faster cooling rate leads to the formation of finer grains, particularly in the bottom region, where the microhardness is markedly higher [34]. This refinement in grain structure enhances the weldment's hardness and overall mechanical properties.

As observed in the microstructural analysis, the presence of equiaxed grains and the reduction of coarse grain structures in the PCTIG weldment further support the improved hardness profile. The controlled diffusion of alloying elements during the cyclic heating and cooling process ensures a more homogeneous distribution, reducing the likelihood of segregation and contributing to the increased hardness values. In both CCTIG and PCTIG weldments, the base metal exhibits higher hardness values compared to the heat-affected zone (HAZ) and fusion zone [35]. This higher hardness can be attributed to the more excellent chemical and microstructural uniformity of the base metal, which has not undergone the thermal cycles and potential elemental segregation experienced by the weld zones.

3.2.2. Tensile test properties

The tensile strength and ductility of weld joints created by Constant Current TIG (CCTIG) and Pulsed Current TIG (PCTIG) welding processes were evaluated through tensile testing. Figure 6 illustrate the stress-strain diagrams for both welding methods. For the CCTIG weldment, the average tensile strength is 737 MPa, and the elongation is 56.75%. For the PCTIG weldment, the average Tensile Strength is 742 MPa and the Elongation is 53.5%. The tensile test results indicate that both CCTIG and PCTIG weldments exhibit high tensile strength, surpassing the strength of the base metal. The fracture in both cases occurred in the base metal, which suggests that the weld joints are stronger than the surrounding material. This outcome is a positive indicator of the weld quality, implying that the welding process did not introduce significant weaknesses into the joint.

The higher tensile strength and ductility observed in PCTIG weldments can be attributed to the microstructural refinement achieved through pulsed current welding. The regulated heat input and appropriate pulse frequency in PCTIG welding promote the formation of finer grains and more uniform microstructures. This refinement enhances the mechanical properties by increasing the material's resistance to deformation and fracture. The slightly higher tensile strength in PCTIG weldments (742 MPa) compared to CCTIG weldments (737 MPa) reflects the benefits of the pulsed current technique. The cyclic heating and cooling during PCTIG welding produces a more homogeneous distribution of alloying elements and reduced grain size, contributing to increased strength.

The stress-strain diagrams shown in Figure 6 provide further insights into the mechanical behavior of the weldments. CCTIG and PCTIG weldments exhibit typical ductile fracture characteristics, with substantial elongation before failure. The elongation

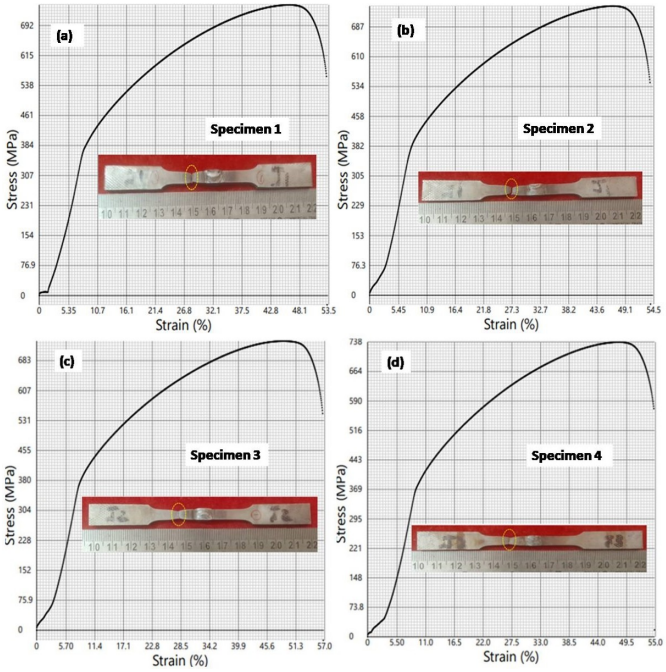

Fig 6. Stress-Strain Curve for the similar weldments of SMO 254 using ERNiCrMo-3 filler (a) & (b) CCTIG (c) & (d) PCTIG

values indicate that the weldments can undergo significant plastic deformation, which is crucial for applications requiring high toughness and resistance to impact loads[36]. The higher elongation observed in CCTIG weldments (56.75%) compared to PCTIG weldments (53.5%) suggests that the continuous current welding process allows for greater ductility. However, the trade-off is a slightly lower tensile strength due to coarse grains and potential elemental segregation.

The Charpy V-notch impact test evaluated the joint toughness of weldments created by Constant Current TIG (CCTIG) and Pulsed Current TIG (PCTIG) welding processes. The results, presented in terms of impact toughness, provide critical insights into the ability of the weldments to absorb energy and resist fracture under dynamic loading conditions. For the CCTIG weldment the Impact Toughness is 81 MPa and for PCTIG weldment is 131 MPa. The impact toughness results indicate a significant difference in the energy absorption capabilities of the weldments produced by the two welding techniques. The PCTIG weldments exhibit substantially higher impact toughness (131 MPa) compared to the CCTIG weldments (81 MPa), highlighting the pulsed current technique's superior performance in enhancing the weld joints' toughness.

The fracture surfaces observed following the impact tests reveal distinct differences between the two welding methods. In the CCTIG weldments, the specimens were completely ruptured upon impact, indicating a lower resistance to fracture and less energy absorption capability. The total rupture of the CCTIG weldments suggests that the microstructure was less capable of withstanding the dynamic load, leading to a brittle fracture mode. The enhanced toughness observed in PCTIG weldments can be attributed to the microstructural refinement achieved through the pulsed current welding process[37]. The regulated heat input and controlled cooling rates associated with PCTIG welding promote the formation of finer grains and a more homogeneous microstructure. The presence of fine equiaxed grains and reduced segregation of alloying elements, as previously discussed, contributes to the improved toughness of the weldments.

The primary austenite phase in the weld metal, observed in both CCTIG and PCTIG weldments, plays a significant role in the toughness of the joints. Austenite is known for its excellent toughness and ability to undergo significant plastic deformation. The improved toughness in PCTIG weldments is likely due to the refined austenitic microstructure, which enhances the material's ability to absorb energy and resist fracture[38]. Both CCTIG and PCTIG weldments exhibit significant plastic deformation before fracture, as evidenced by the fracture surfaces. The PCTIG weldments show more ductile behavior, remaining mostly intact and absorbing more energy, while the CCTIG weldments undergo brittle fracture, with complete rupture occurring at lower energy levels.

3.2.3. Impact Test Fractography

The SEM analysis of the CCTIG weldment fracture surface, depicted in Figure 7 **(a),** reveals serrated facets with numerous microvoids. These features suggest a mixed mode of failure that includes both brittle and ductile characteristics. Serrated facets indicate that the fracture propagated along specific crystallographic planes, a typical feature of brittle fracture. The microvoids observed within these facets indicate localized plastic deformation, where voids nucleate, grow, and coalesce under the influence of stress. The fractography features of the CCTIG weldment suggest that fatigue may have influenced the failure. During the Charpy impact test, the repeated cyclic loading could have initiated and propagated cracks along the serrated facets, leading to microvoids and eventual fracture. The fatigue-induced microvoids are consistent with the observed lower impact toughness of the CCTIG weldments, which show a complete rupture during impact testing.

In contrast, the SEM analysis of the PCTIG weldment fracture surface, shown inFigure 7**(b),** reveals a predominance of microvoids and equiaxed dimples. These features are characteristic of a ductile mode of failure, where the material undergoes significant plastic deformation before fracture. The equiaxed dimples are formed due to microvoids' nucleation, growth, and coalescence under tensile stress, indicating that the material absorbed a substantial amount of energy before failing. The ductile fracture mode observed in the PCTIG weldment is attributed to the intermittent heating and cooling during the pulsed current welding process[39]. This thermal cycling promotes the formation of a refined microstructure with fine equiaxed grains and reduces the segregation of alloying elements such as Nb and Mo. The homogeneous distribution of these elements enhances the material's ability to deform plastically and absorb impact energy, resulting in higher impact toughness and better fracture resistance[40].

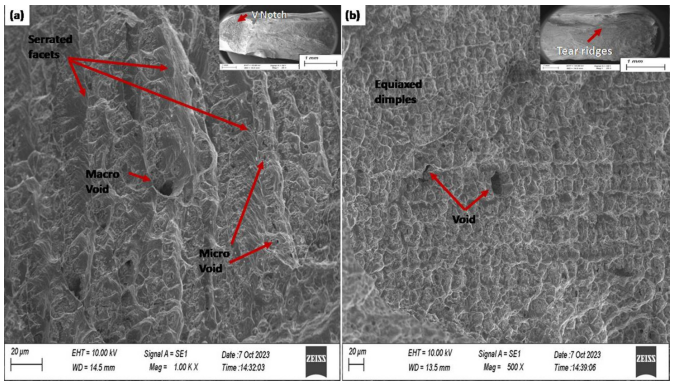

Fig 7. Impact-tested specimen fractography of (a) CCTIG (b) PCTIG

In CCTIG weldments, the continuous heat input leads to coarser grain structures and potential segregation of alloying elements, contributing to the mixed failure mode with serrated facets and microvoids. Nb and Mo segregations at grain boundaries can act as stress concentrators, facilitating crack initiation and propagation under cyclic loading conditions. In PCTIG weldments, the pulsed current technique promotes the formation of fine equiaxed grains and minimizes the segregation of alloying elements[41]. The refined microstructure and uniform elemental distribution enhance the material's toughness and ductility, as evidenced by equiaxed dimples on the fracture surface. The reduced segregation of Nb and Mo prevents the formation of localized stress concentrators, thereby improving the material's resistance to impact loading.

The fractography analysis highlights the superior fracture resistance of PCTIG weldments compared to CCTIG weldments. The ductile failure mode observed in PCTIG weldments, characterized by equiaxed dimples and microvoids, indicates a higher capacity for energy absorption and plastic deformation[42]. This enhanced toughness and ductility are crucial for applications where weld joints are subjected to dynamic loads and impact stresses[43].

3.3Corrosion characteristics

The electrochemical corrosion behavior of weldments created by Constant Current TIG (CCTIG) and Pulsed Current TIG (PCTIG) welding techniques was evaluated through polarization studies. Figure 8 **(a)** and **(b)** displays the polarization graphs, and key parameters such as corrosion current (I_{corr}), corrosion potential (E_{corr}), and corrosion rate (CR) were measured to understand the corrosion performance of both welding methods. For CCTIG weldment, I_{corr} is 546.551 nA/cm^2 and E_{corr} is -2.907 mV. The CCTIG weldment features coarse grains with fewer grain boundaries. Coarse grains reduce the number of active sites for corrosion, as grain boundaries are typically more susceptible to corrosive attack than the grain interiors. The lower

number of grain boundaries in the CCTIG weldment contributes to its slightly lower corrosion rate and less negative corrosion potential. This microstructure limits the overall corrosion activity, resulting in a more stable and less reactive weldment under electrochemical conditions. For CCTIG weldment is Corrosion Rate (CR): 0.23106 mpy and for PCTIG weldment is 0.23362 mpy.

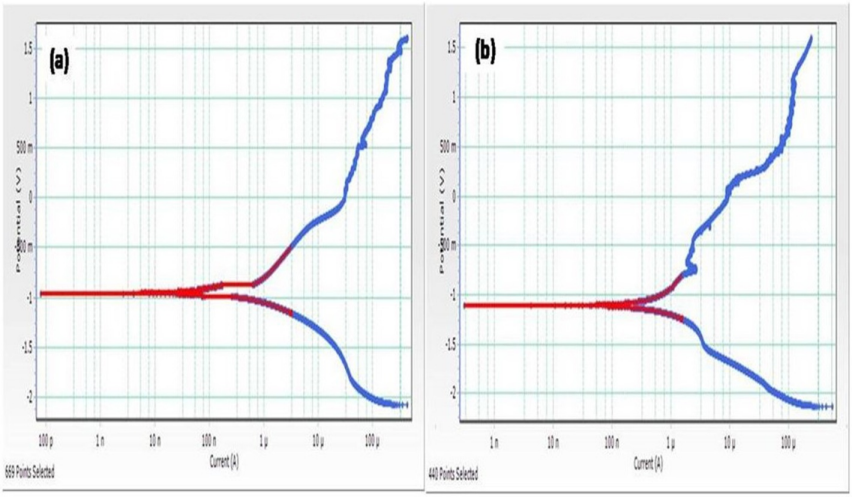

Fig 8. Potentiodynamic polarization curves of ERNiCrMo-3 fillers (a) CC-TIG (b) PC-TIG

For PCTIG weldment, I_{corr} is 552.589 nA/cm^2 and E_{corr} is -950.451 mV. PCTIG weldment exhibits a finer grain structure with a higher density of grain boundaries. While finer grains generally enhance mechanical properties such as toughness and strength, they can also increase the susceptibility to corrosion. Grain boundaries act as preferential sites for corrosion initiation due to their higher energy state and potential for impurity segregation[44]. The increased grain boundaries in the PCTIG weldment leads to higher corrosion activity, as reflected by the more negative E_{corr} value and the slightly higher corrosion rate. The intermittent heating and cooling during the pulsed current welding process promote the formation of these finer grains, enhancing both the mechanical properties and the susceptibility to corrosion[45].

While PCTIG welding enhances the mechanical properties through microstructural refinement, it also introduces a higher density of grain boundaries, which can act as active sites for corrosion. This results in a marginally higher corrosion rate than CCTIG weldments[46]. Despite the higher corrosion rate in PCTIG weldments, the overall corrosion rates for both welding techniques are relatively low, indicating good corrosion resistance of the weld joints in general[47]. The choice between CCTIG and PCTIG welding should consider the specific application requirements, balancing the need for superior mechanical properties with acceptable corrosion resistance.

4 Conclusions

- CCTIG and PCTIG welding methods produce similar dilution percentages, with PCTIG showing a slightly higher dilution percentage of 38.00% compared to CCTIG's 36.50%. CCTIG weldments exhibit coarse grains and fewer grain boundaries, resulting in more uniform microstructures. In contrast, PCTIG weldments show finer grains and more grain boundaries due to the regulated heat input and pulse frequency.
- PCTIG weldments exhibit higher microhardness in the bottom region (265.46 HV) compared to the top (221.73 HV) and middle (224.3 HV), attributed to the faster cooling rate and refined grain structure. Microhardness values are higher in the bottom region of PCTIG weldments due to faster cooling rates and grain refinement.
- Both CCTIG and PCTIG weldments exhibit high tensile strength, with CCTIG at 737 MPa and PCTIG at 742 MPa. Elongation values are higher for CCTIG weldments (56.75%) than PCTIG weldments (53.5%), indicating greater ductility in CCTIG weldments. PCTIG weldments remain mostly intact after impact testing, indicating higher resistance to fracture and better energy absorption than CCTIG weldments, which exhibit total rupture.
- Corrosion rate (CR) is slightly higher for PCTIG weldments (0.23362 mpy) compared to CCTIG weldments (0.23106 mpy), attributed to the increased density of grain boundaries in PCTIG weldments. Despite a slightly higher corrosion rate, PCTIG weldments show good overall corrosion resistance, balancing the need for superior mechanical properties

with acceptable corrosion resistance.

References

1) Singh R. pplied Welding Engineering, Processes, Codes and Standards. In: Welding, corrosion-resistant alloys-Stainless steel. *Butterworth-Heinemann*. Available from: https://doi.org/10.1016/C2019-0-03490-5.
2) Bansod A, Shukla S, Gahiga G, Verma J. Influence of filler wire on metallurgical, mechanical, and corrosion behaviour of 430 ferritic stainless steel using a fusion welding process. *Materials Research Express*. 2023;10(036513):1–13. Available from: https://doi.org/10.1088/2053-1591/acb908.
3) Roshith P, Arivarasu M, Arivazhagan N, Srinivasan A, Prabhakar PKV. Investigations on induced residual stresses, mechanical and metallurgical properties of CO2 laser beam and pulse current gas tungsten arc welded SMO 254. *Journal of Manufacturing Process*. 2019;44. Available from: https://doi.org/10.1016/j.jmapro.2019.05.044.
4) Sivakumar N, Gandhi BS, Kumar KS, Arulmurugan B. Effect of constant current and pulsed current gas tungsten arc welding process on microstructure and mechanical properties of super alloy 59 joints. *Materials Research Express*. 2022;9(046525):1–21. Available from: https://doi.org/10.1088/2053-1591/ac6793.
5) Tembhurkar C, Katria R, Ambade S, Verma J. Anand Sharma & Saurabh Sarkar, "Effect of fillers and Autogenous welding on dissimilar welded 316L Austenitic and 430 Ferritic Stainless steels". *Journal of Materials Engineering and Performance*. 2021;30:1444–1453. Available from: https://doi.org/10.1007/s11665-020-05395-4.
6) Kumar MK, Arivzhagan N, Kuppan P. Studies on the effect of filler on micro level segregation of alloying elements in the alloy 617 weld fusion zone". *Materials Research Express*. 2019;(6):1–15. Available from: https://doi.org/10.1088/2053-1591/ab4946.
7) Yelamasetti B, Rajyalakshmi G, Ramana VG, Babu SB, Vemanabonia H. Comparison of metallurgical and mechanical properties of dissimilar joint of AISI 316 and Monel 400 developed by pulsed and constant current gas tungsten arc welding processes. *The International Journal of Advanced Manufacturing Technology*. 2020;108:2633–2644. Available from: https://doi.org/10.1007/s00170-020-05562-w.
8) Aghayar Y, Naghashzadeh A, Atapour M. n assessment of microstructure and mechanical properties of Inconel 601/304 stainless steel dissimilar weld", . *VAVACCUM*. 2021;184:1–10. Available from: https://doi.org/10.1016/j.vaccum.2020.109970.
9) Khan MFZ, Junaid M, Hassan AA, Baig MN. Effect of pulsation in TIG welding on the microstructure, residual stresses, tensile and impact properties of Ti-5Al-2.5Sn alloy. *Journal of PROCESS MECHANICAL ENGINEERING*. 2020. Available from: https://doi.org/10.1177/0954408920964689.
10) Shanmugasundar G, Bansod A, Schindlerova V, Cep R. Influence of Filler Material on the Microstructural and Mechanical Properties of 430 Ferritic Stainless Steel Weld Joints,. *materials*. 2023;16:1–12. Available from: https://doi.org/10.3390/ma16041590.
11) Ramarajan A, Jayakumar K. Influence of pulsed TIG welding process Parameters on the mechanical characteristics of AA5083 with AA6082 weldments. *Materials Research Express*. 2023;10. Available from: https://doi.org/10.1088/2053-1591/acb682.
12) Yusof MFM, Ishak M, Ghazali MF. Weld depth estimation during pulse mode laser welding process by the analysis of the acquired sound using feature extraction analysis and artificial neural network. *Journal of Manufacturing Processes*. 2021;63:163–178. Available from: https://doi.org/10.1016/j.jmapro.2020.04.004.
13) Uribe AMM, Vaccari L, Bracarense AQ, Maier HJ, Hassel T. Operational performance and metal droplet formation in pulsed-shielded metal arc underwater welding. *Archives of Civil and Mechanical Engineering*. 2024;24. Available from: https://doi.org/10.1007/s43452-024-00916-7.
14) Wang X, Wang C, Kang J, Yuan G, Misra RDK, Wang G. Improved toughness of double-pass welding heat affected zone by fine Ti-Ca oxide inclusions for high-strength low-alloy steel. *Materials Science and Engineering: A*. 2020;780. Available from: https://doi.org/10.1016/j.msea.2020.139198.
15) Kuang X, Qi B, Zheng H. Effect of pulse mode and frequency on microstructure and properties of 2219 aluminum alloy by ultrahigh-frequency pulse Metal-Inert Gas Welding. *Journal of Materials Research and Technology*;20:3391–3407. Available from: https://doi.org/10.1016/j.jmrt.2022.08.094.
16) Sabzi M, Anijdan SHM, Eivani AR, Park N, Jafarian HR. The effect of pulse current changes in PCGTAW on microstructural evolution, drastic improvement in mechanical properties, and fracture mode of dissimilar welded joint of AISI 316L-AISI 310S stainless steels. *Materials Science and Engineering: A*. 141700;823. Available from: https://doi.org/10.1016/j.msea.2021.141700.
17) Yelamasetti B, Vardhan TV, Ramana G. Study of metallurgical changes and mechanical properties of dissimilar weldments developed by interpulse current TIG welding technique. *Proceedings of Institution of Mechanical Engineers*. 2021;235:2985–2997. Available from: https://doi.org/10.1177/0954406220960780.
18) Rathore S, Kumar A, Sirohi S, Singh V, Gupta A, Fydrych D, et al. Role of buttering layer composition on microstructural heterogeneity and mechanical properties of Alloy 617 and P92 steel dissimilar welded joints for future Indian AUSC program. *The International Journal of Advanced Manufacturing Technology*. 2024;133(1-2):671–700. Available from: https://dx.doi.org/10.1007/s00170-024-13747-w.
19) Yelamasetti B, Rajyalakshmi G. Residual stress analysis, mechanical and weldments metallurgical of Monel properties 400 and AISI dissimilar 316. *International Journal of Materials Research*. 2020;111. Available from: https://doi.org/10.3139/146.111961.
20) Sommer N, Stredak F, Wiegand M, Bohm S. Grain growth and precipitation behaviour of AISI 430 ferritic stainless steel subjected to pulsed laser beam welding using free-form pulse shaping. *Welding in the World*. 2023;67:51–62. Available from: https://doi.org/10.1007/s40194-022-01398-y.
21) RTabrizi T, Sabzi M, Anijdan SHM, Eivani AR, Park N, Jafarian HR. Comparing the effect of continuous and pulsed current in the GTAW process of AISI 316L stainless steel welded joint: microstructural evolution, phase equilibrium, mechanical properties and fracture mode. *Journal of Materials Research and Technology*. 2021;15:199–212. Available from: https://dx.doi.org/10.1016/j.jmrt.2021.07.154. doi:10.1016/j.jmrt.2021.07.154.
22) Yelamasetti B, Adithya GS, Ramadevi RS, Sonia P, Saxena KK, Kumar PN. Metallurgical, mechanical and corrosion behaviour of pulsed and constant current TIG dissimilar welds of AISI 430 and Inconel 718. *Journal of Materials Research and Technology*. 2023;24. Available from: https://doi.org/10.1016/j.jmrt.2023.04.231.
23) Sonar T, Balasubramanian V, Venkateswaran T, Xavier V, Muthumanickam A, Manjunath A, et al. Effect of post weld heat treatment on weld metal microstructure and hardness of HFCA-TIG welded ASTM-B670 high temperature alloy joints. *Journal of Alloys and Metallurgical Systems*. 2023;3:100025–100025. Available from: https://dx.doi.org/10.1016/j.jalmes.2023.100025.
24) Yelamasetti B, Ramana VG, Manikyam S, Vardhan VT. Thermal field and residual stress analyses of similar and dissimilar weldments joined by constant and pulsed current TIG welding techniques. *Advances in Materials and Processing Technologies*. 2022;8(sup3):1889–1904. Available from: https://dx.doi.org/10.1080/2374068x.2021.1959114.
25) Singh A, Singh V, Singh AP, Ashutosh S, Patel D. Welding investigations on mechanical property and microstructure of TIG and A-TIG Weld of Hastelloy C-276. *Engineering Research Express*. 2023;5(2):025004–025004. Available from: https://dx.doi.org/10.1088/2631-8695/acc92a.

26) Giudice F, Missori S, Scolaro C, Sili A. A Review on Fusion Welding of Dissimilar Ferritic/Austenitic Steels: Processing and Weld Zone Metallurgy. *Journal of Manufacturing and Materials Processing*. 2024;8(3):96–96. Available from: https://dx.doi.org/10.3390/jmmp8030096.
27) Goriparthi V, Nallu R, Chebolu R, Indupuri S, Rudrapati R. Experimental Studies on Mechanical Behavior of TIG and Friction Stir Welded AA5083 -AA7075 Dissimilar Aluminum Alloys. *Advances in Materials Science and Engineering*. 2023;2023:1–7. Available from: https://dx.doi.org/10.1155/2023/8622525.
28) Rodrigues CAD, Bandeira RM, Duarte BB, Filho GT, Roche V, Jorge AM. The Influence of Ni Content on the Weldability, Mechanical, and Pitting Corrosion Properties of a High-Nickel-Bearing Supermartensitic Stainless Steel. *Journal of Materials Engineering and Performance*. 2021;30(4):3044–3053. Available from: https://dx.doi.org/10.1007/s11665-021-05600-y.
29) Zhang C, Hu Q, Wang X, Dong Z, Du D. INFLUENCE OF VOLTAGE AND CURRENT ON THE ARC SHAPE IN CABLE-TYPE WIRE TIG-MIG HYBRID WELDING. . *Materiali in Tehnologije 2022*;56. Available from: https://doi.org/10.17222/mit.2021.340.
30) Habba MI, Alsaleh NA, Badran TE, Seleman MME, Ataya S, El-Nikhaily AE, et al. Comparative Study of FSW, MIG, and TIG Welding of AA5083-H111 Based on the Evaluation of Welded Joints and Economic Aspect. *Materials*. 2023;16(14):5124–5124. Available from: https://dx.doi.org/10.3390/ma16145124.
31) Shravan C, Radhika N, Kumar NH, Sivasailam B. A review on welding techniques: properties, characterizations and engineering applications. *Advances in Materials and Processing Technologies*. 2024;10:1126–1181. Available from: https://doi.org/10.1080/2374068X.2023.2186638.
32) Mutaşcu D, Karancsi O, Mitelea I, Crăciunescu CM, Buzdugan D, Uțu ID. Pulsed TIG Cladding of a Highly Carbon-, Chromium-, Molybdenum-, Niobium-, Tungsten- and Vanadium-Alloyed Flux-Cored Wire Electrode on Duplex Stainless Steel X2CrNiMoN 22-5-3. *Materials*. 2023;16(13):4557–4557. Available from: https://dx.doi.org/10.3390/ma16134557.
33) Casanueva R, Brañas C, Diaz FJ, Azcondo FJ, Ferreño D, Setien J. Characterization of an energy efficient pulsed current TIG welding process on AISI 316 and 304 stainless steels. *Heliyon*. 2023;9. Available from: https://doi.org/10.1016/j.heliyon.2023.e19819.
34) Cui J, Li N, Yan J, Zhou L, Lin R, Qu Y. Increase in Mechanical Properties and Damping Capacity of a Cast Mn-Cu Damping Alloy Welded Joint by Pulsed Current TIG Welding. *J Mater Eng Perform*. 2022;31. Available from: https://doi.org/10.1007/s11665-022-07001-1.
35) Wu J, Wang Z, Zhu Z, Fan W, Lin S, Cai X. Effect of Fast-Frequency Pulsed Current Parameters on FFP-TIG Arc Behavior and Its Implications for Inconel 718 Welding. *Metals (Basel)*. 2023;13. Available from: https://doi.org/10.3390/met13050848.
36) Mician M, Fratrik M, Bruna M. Softening effect in the heat-affected zone of laser-welded joints of high-strength low-alloyed steels. *Welding in the World*. 2024;68:1497–1514. Available from: https://doi.org/10.1007/s40194-024-01730-8.
37) Yelamasetti B, Ss N, Saxena KK, Gupta N, Nk P, Shelare SD. Metallurgical, mechanical and corrosion behavior of Interpulse and pulsed current TIG dissimilar welds of Monel 400 and AISI 316L. *Proceedings of the Institution of Mechanical Engineers*. 2023. Available from: https://doi.org/10.1177/09544089231216029.
38) Wu J, Wang Z, Lin S, Xie Z, Xu M, Tian J, et al. Effect of fast-frequency pulse waveforms on the microstructure and mechanical properties of Ti-6Al-4V alloy welded by FFP-TIG. *Journal of Materials Research and Technology*;20:516–531. Available from: https://doi.org/10.1016/j.jmrt.2022.07.126.
39) Liu S, Ji H, Zhao W, Hu C, Wang J, Li H, et al. Evaluation of Arc Signals, Microstructure and Mechanical Properties in Ultrasonic-Frequency Pulse Underwater Wet Welding Process with Q345 Steel. *Metals*. 2022;12(12). Available from: https://doi.org/10.3390/met12122119.
40) Ostromęcka M, Kolasa A. The effect of the current pulsation frequency on heat supply results during pulsed current TIG welding in 301L stainless steel. *Welding Technology Review*. 2019;91. Available from: https://doi.org/10.26628/wtr.v91i8.1046.
41) Venkatesh R, Manivannan S, Kaliappan S, Socrates S, Sekar S, Patil PP. Influence of Different Frequency Pulse on Weld Bead Phase Ratio in Gas Tungsten Arc Welding by Ferritic Stainless Steel AISI-409L. *J Nanomater*. 2022;2022. Available from: https://doi.org/10.1155/2022/9530499.
42) Generoso VMA, Souza LM, De, Pereira EC, Monteiro SN, Azevedo AD. Influence of Pulsed Arc Parameters on the Tig Welding Process for the Stainless Steel Duplex UNS S31803. *Materials*. 2023;16. Available from: https://doi.org/10.3390/ma16216870.
43) Kumar P, Kumar R, Arif A, Veerababu M. Investigation of numerical modelling of TIG welding of austenitic stainless steel (304L). *Mater Today Proc*. 2020;27. Available from: https://doi.org/10.1016/j.matpr.2020.03.544.
44) Soleimani M, Mirzadeh H, Dehghanian C. Effect of grain size on the corrosion resistance of low carbon steel. *Materials Research Express*. 2020. Available from: https://doi.org/10.1088/2053-1591/ab62fa.
45) Chuaiphan W, Srijaroenpramong L, Microstructure. mechanical properties and pitting corrosion of TIG weld joints alternative low-cost austenitic stainless steel grade 216. *Journal of Advanced Joining Processes*. 2020;2. Available from: https://doi.org/10.1016/j.jajp.2020.100027.
46) Touileb K, Djoudjou R, Hedhibi AC, Ouis A, Benselama A, Ibrahim A. Comparative Microstructural, Mechanical and Corrosion Study between Dissimilar ATIG and Conventional TIG Weldments of 316L Stainless Steel and Mild Steel. . *Metals (Basel) 2022*;12. Available from: https://doi.org/10.3390/met12040635.
47) Pinheiro FW, De Souza LM, Pereira EC, Monteiro SN, Azevedo ARG. Effect of solubilization heat treatment on microstructure and corrosion resistance of joints welded with the autogenous TIG process duplex stainless steel. *Journal of Materials Research and Technology*. 2023;26. Available from: https://doi.org/10.1016/j.jmrt.2023.08.014.